JACS
JOURNAL OF THE AMERICAN CHEMICAL SOCIETY

Article

pubs.acs.org/JACS

Shape Fixing via Salt Recrystallization: A Morphology-Controlled Approach To Convert Nanostructured Polymer to Carbon Nanomaterial as a Highly Active Catalyst for Oxygen Reduction Reaction

Wei Ding, Li Li, Kun Xiong, Yao Wang, Wei Li, Yao Nie, Siguo Chen, Xueqiang Qi, and Zidong Wei*

Chongqing Key Laboratory of Chemical Process for Clean Energy and Resource Utilization, School of Chemistry and Chemical Engineering, Chongqing University, Shazhengjie 174, Chongqing 400044, China

Supporting Information

ABSTRACT: Herein, we report a "shape fixing via salt recrystallization" method to efficiently synthesize nitrogen-doped carbon material with a large number of active sites exposed to the three-phase zones, for use as an ORR catalyst. Self-assembled polyaniline with a 3D network structure was fixed and fully sealed inside NaCl via recrystallization of NaCl solution. During pyrolysis, the NaCl crystal functions as a fully sealed nanoreactor, which facilitates nitrogen incorporation and graphitization. The gasification in such a closed nanoreactor creates a large number of pores in the resultant samples. The 3D network structure, which is conducive to mass transport and high utilization of active sites, was found to have been accurately transferred to the final N-doped carbon materials, after dissolution of the NaCl. Use of the invented cathode catalyst in a proton exchange membrane fuel cell produces a peak power of 600 mW cm^{-2}, making this among the best nonprecious metal catalysts for the ORR reported so far. Furthermore, N-doped carbon materials with a nanotube or nanoshell morphology can be realized by the invented method.

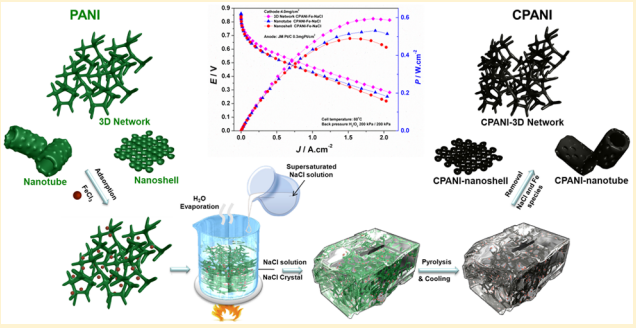

INTRODUCTION

Proton exchange membrane fuel cells (PEMFCs) are electrochemical power generators, with potential applications in vehicle propulsion. To reduce their cost and encourage widespread use, researchers have focused on replacing the expensive Pt-based electrocatalyst with a lower-cost alternative for catalysis of the oxygen reduction reaction (ORR) on the cathode side of the cells.[1] Great efforts have been undertaken to produce nonprecious metal catalysts (NPMCs) by pyrolyzing nitrogen-containing precursors on a carbon support material.[2] However, the power densities of these NPMC-based cathodes have been low compared with those of Pt-based cathodes, due to fewer active sites and poor mass-transport properties.[3]

One widely used strategy for the introduction of adequate active sites is to increase the surface area of the NPMCs by using hard or soft template methods.[4] However, the template methods frequently fail in increasing the number of ORR active sites because the templates hinder contact between the nitrogen-containing precursors and metals, which is needed to induce or catalyze the transformation of nitrogen-containing precursors into materials that can catalyze the ORR. To increase precursor−metal contact in template methods, an advanced template strategy has been developed by using a low volatility precursor to form more N-containing active centers at the precursor's molten state.[5] The fuel cell with this template synthesized catalyst cathode produced a power of 420 mW cm^{-2}. Recently, with pyrolysis of well-defined metal−ligand coordinated metal−organic frameworks (MOFs) or porous organic polymers (POPs), NPMCs were produced with surface areas of up to 903 m^2 g^{-1} and an initial performance of close to the level reached by platinum-based catalysts.[6] In addition to the number of active sites, the exposure of the active sites to the interface, where electrons, protons, oxygen, and product water can flow in or exit out, is particularly important. Otherwise, the active sites cannot be utilized by the ORR.[7] Therefore, it would be better if the NPMCs were porous enough or had enough space to accommodate the linkage of various species-transport channels to their active sites: voids for O_2 and water, a polymer chain for protons, and a carbon framework for electrons. At this point, the traditional direct pyrolysis of the mixture of nitrogen-containing compounds, carbon, and transition metal precursors frequently fails in producing the necessary porous structure, leading to relatively poor transport properties and limited active sites that are accessible for the ORR.[3,8] Recently, we reported a space-confinement-induced method to selectively synthesize planar pyridinic and pyrrolic N-doped graphene.[9] It exhibited a high yield of planar pyridinic and pyrrolic N-doped graphene

Received: January 10, 2015
Published: April 14, 2015

DOI: 10.1021/jacs.5b00292
J. Am. Chem. Soc. 2015, 137, 5414−5420

Scheme 1. Shape Fixing via Salt Recrystallization Method

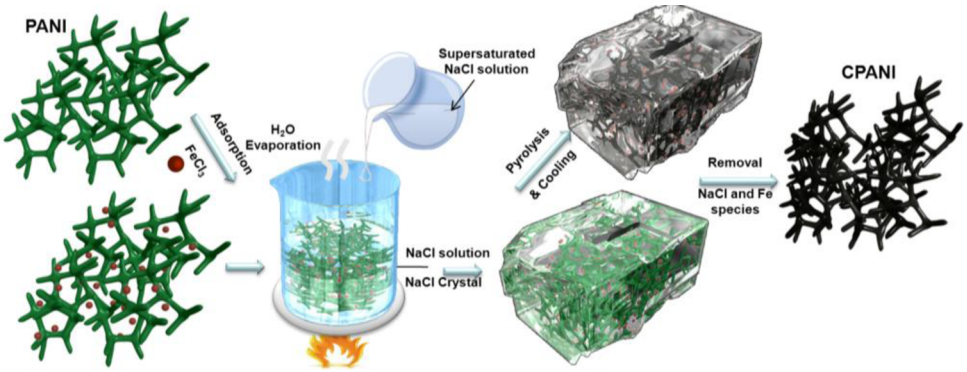

and acceptable ORR catalysis. The density of the exposed sites activated by planar pyridinic and pyrrolic N, however, is still not high enough, as the exposed active sites only appear at the fringe of a large sheet of graphene.

Herein, we report a "shape fixing via salt recrystallization method" to efficiently synthesize N-doped carbon material, with many active sites exposed to the three-phase zones, as a catalyst for the ORR. The procedure is shown in Scheme 1. A 3-dimensional (3D) PANI network was fabricated via a self-assembly process. (Unless otherwise stated, PANI refers to the 3D PANI network.) After adsorption of $FeCl_3$, an 80 °C, supersaturated NaCl solution was poured into a beaker containing PANI. The water was then evaporated so that the NaCl recrystallized around the PANI on the bottom of the beaker. This cycle of the addition of NaCl solution, water evaporation, and NaCl recrystallization was repeated until the whole PANI was fully buried so that it appeared to be tightly sealed inside the NaCl crystal. Thus, the original shape of the 3D PANI network would be fixed by NaCl crystal. After the NaCl crystal-sealed PANI was dehydrated at 120 °C, the temperature was raised to 900 °C at a heating rate of 6 K min^{-1}, held at 900 °C for 3 h under flowing N_2, and finally cooled down to room temperature. The NaCl crystal and iron species were washed off in a hot 0.5 M H_2SO_4 solution. The resultant sample is referred to as CPANI-Fe-NaCl. For comparison, samples obtained from pyrolysis using NaCl crystal only, and those without either $FeCl_3$ or NaCl, were termed as CPANI-NaCl and CPANI, respectively. In this process, the NaCl crystal serves as a fully closed nanoreactor, which facilitates the N incorporation and graphitization. Moreover, when the temperature reaches 800.9 °C, i.e., the melting temperature of NaCl, the NaCl molten salt can facilitate the formation of active sites. The original 3D structure of the PANI is well-preserved, and various pores, from micro- to meso- to macrosized, are formed in large quantities in the high temperature pyrolysis, due to the gasification of various raw materials in a closed space. Electrochemical evaluations showed that the invented catalyst exhibits excellent conductivity, high ORR activity, and good stability in acidic electrolytes. In the present work the half-wave potential of the ORR on an electrode made of the invented catalyst was found to lag behind the state-of-the-art carbon-supported platinum by only 58 mV in acid electrolyte. The PEMFC, prepared with the invented catalyst as the cathode, achieved a maximum power density of 600 mW cm^{-2}. It is demonstrated that N-doped carbon materials with 3D network morphology, nanotubes and nanoshells, can be realized by the shape fixing via salt recrystallization method. To our knowledge, this is the first report of such a method to efficiently construct carbon nanomaterials for catalysis of the ORR with controlled porous structure, active sites, and morphology.

EXPERIMENTAL SECTION

Synthesis of PANI 3D Networks. Aniline monomer was distilled under reduced pressure before use. The PANI 3D network was synthesized by a slow chemical oxidation and self-assembly polymerization. In a typical synthesis, 3.728 g of aniline and 0.554 g of salicylic acid (SA) were dissolved in 200 mL of deionized water with magnetic stirring at room temperature for 24 h. The stirring was then stopped. After 10 min, a 50 mL aqueous solution of 9.294 g of ammonium persulfate (APS) was added at an addition rate of 0.8 mL/min, and the reaction was left for 48 h. The resulting PANI was washed with water, methanol, and ether several times. Finally, the product was dried under vacuum at room temperature for 24 h.

Synthesis of PANI Nanotubes and PANI Nanoshells. The PANI nanotubes and PANI nanoshells were synthesized by a severe chemical oxidation and self-assembly polymerization, similar to that reported previously.[10] Aniline (3.725 g) and SA (1.379 g for nanotubes, 3.408 g for nanoshells) were dissolved in deionized water (200 mL). APS (9.320 g) was also dissolved in deionized water (20 mL) in a separate vial. The two solutions were vigorously mixed at room temperature. A brown precipitate appeared immediately, and the subsequent reaction was carried out at room temperature without any disturbance. After 7 days, the precipitate was filtered and purified using a Buchner funnel with a water aspirator to wash the product several times with water, methanol, and ether. Finally, the product was dried in vacuum at room temperature for 24 h.

Preparation of CPANI-Fe-NaCl by the Salt Crystallization Method. Typically, 0.6 g of PANI and 0.6 g of $FeCl_3 \cdot 6H_2O$ were suspended in 10 mL of deionized water, with magnetic stirring, at room temperature, for 12 h. After the adsorption of $FeCl_3$, 15 mL of supersaturated NaCl solution was added to the suspension, and magnetic stirring was continued for 2 h. The suspension was raised to 60 °C to evaporate off water. During the evaporation, an 80 °C oversaturated NaCl solution was continually and slowly added into the suspension, until the NaCl crystallized, encasing the PANI. To minimize the creation of air pockets during evaporation, the sample was repeatedly transferred to a vacuum chamber and held at a pressure of −0.1 MPa at 60 °C for 1 h after addition of a small amount of 80 °C supersaturated NaCl solution. The composite was then dried under vacuum at 60 °C for 24 h. The composite was then heated to 120 °C, after which the temperature was raised to 900 °C at a heating rate of 6 K min^{-1} and held at 900 °C for 3 h under flowing N_2. The NaCl crystal and iron species in the sample were finally washed off in 0.5 M H_2SO_4 solution at 80 °C.

Synthesis of CPANI and CPANI-NaCl. The CPANI-NaCl was prepared under conditions similar to those used for CPANI-Fe-NaCl. For CPANI-NaCl, Fe salt was not used, and NaCl was washed with room temperature water. For CPANI, PANI was directly pyrolyzed, without application of the NaCl crystallization procedure.

DOI: 10.1021/jacs.5b00292
J. Am. Chem. Soc. 2015, 137, 5414−5420

RESULTS AND DISCUSSION

The shape fixing via salt recrystallization procedure was monitored by nitrogen adsorption−desorption at 77 K. As shown in Figure 1, the adsorption hysteresis loop for PANI

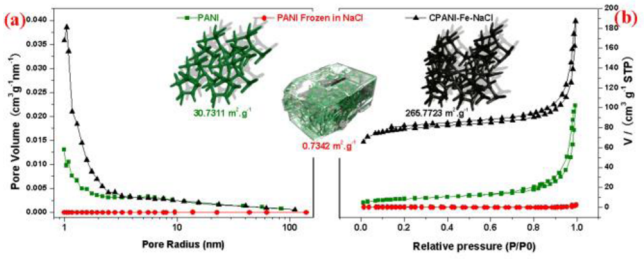

Figure 1. (a) Pore size distribution for PANI, PANI in NaCl, and CPANI-Fe-NaCl, assessed by BJH. (b) Nitrogen sorption isotherms for PANI, PANI in NaCl, and CPANI-Fe-NaCl.

suggests a mesoporous structure, with a pore size distribution centered at 50.0 nm (via the Barrett−Joyner−Halenda method, BJH). After being encased in NaCl crystal, the PANI displays a very small area by Brunauer−Emmett−Teller (BET) theory (0.7 $m^2\ g^{-1}$) compared to the original value (30.7 $m^2\ g^{-1}$). The pore volumes of the NaCl-buried PANI approach zero for all pore radii, indicating that the PANI was fully encapsulated by the NaCl crystal. After pyrolysis at 900 °C and removal of the NaCl crystal in a hot 0.5 M H_2SO_4 solution, the BET surface area of the final CPANI-Fe-NaCl increased to 265.7 $m^2\ g^{-1}$. The BET surface increase is mainly due to the formation of micropores after pyrolysis. As shown in Figure 1a, the pore volumes for those radii ranging from 100 to 2.5 nm are unchanged by the transition from PANI to CPANI-Fe-NaCl, while pore volumes of less than 2.5 nm experience a substantial change. These results indicate that the 3D structure was well-preserved and vast numbers of micropores were formed in the shape fixing via salt recrystallization method.

Figure 2a shows that the PANI 3D networks were composed of PANI nanofibers with a diameter of ∼100 nm. With the shape fixing via salt recrystallization method, as shown in Figure 2b, the PANI 3D network morphologies were faithfully transferred to the 3D carbon networks (see also Supporting Information Figure S1a,b). In contrast, the TEM and SEM images of CPANI synthesized by traditional pyrolysis reveal a large-scale, spherical, or lump-type morphology (see Supporting Information Figure S2a,b). Only one tiny difference can be observed between the morphology of the PANI 3D network and that of the carbon 3D network; that is, there are raised knots on the surface of the PANI but concavities on the CPANI-Fe-NaCl. This further demonstrated that a carbon nanotube with a diameter of ∼200 nm, length of ∼600 nm, and thickness of ∼50 nm (Supporting Information Figure S3a,b), as well as a carbon nanoshell, can be synthesized via the proposed method; all resultant samples accurately inherit their precursors' original structures (Figure 2c−f; see also Supporting Information Figure S1c−f). These excellent conversions demonstrate the high efficiency of the shape fixing via salt recrystallization method in controlling morphology and pore structure. To investigate the role of Fe during the synthesis, we synthesized CPANI-Fe by pyrolyzing PANI absorbed $FeCl_3$. Our results show that Fe ions affect the graphitic structure during the synthesis but they cannot preserve the original shape of PANI. As shown in Supporting Information Figure S4a,b, the

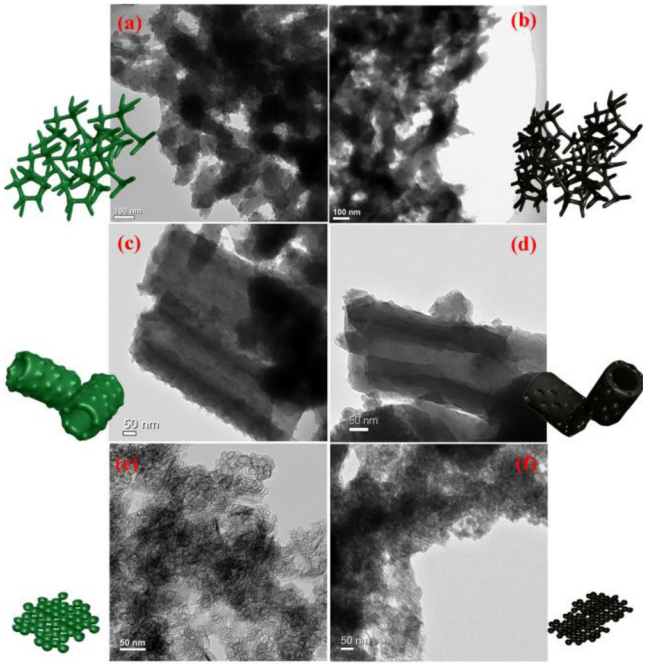

Figure 2. TEM images of as-prepared (a) 3D PANI network, (c) PANI nanotubes, and (e) PANI nanoshell, and their corresponding carbonized products: (b) CPANI-3D-Fe-NaCl, (d) CPANI-NT-Fe-NaCl, and (f) CPANI-NS-Fe-NaCl.

original nanofiber morphology of PANI transforms into a lump-type and graphitic shell-like morphology. The graphitic shell-like morphology does not appear in the case of PANI pyrolysis without Fe participation, i.e., CPANI. The graphitic shells appearing in the CPANI-Fe sample provide evidence that the Fe species catalytically transform PANI into graphitic carbon. In contrast, the CPANI-NaCl preserves network morphology after pyrolysis (Supporting Information Figure S4c) indicating the original shape of PANI can be preserved by NaCl alone.

High resolution transmission electron microscopy (HRTEM), as shown in Figure 3, demonstrated the amorphous carbon structure and lack of lattice fringe of the CPANI. Conversely, the CPANI-NaCl shows relatively clear graphitic fringes, suggesting an improved graphitic structure. This result is also supported by the Raman spectra (see Supporting Information Figure S5), which show the relatively higher

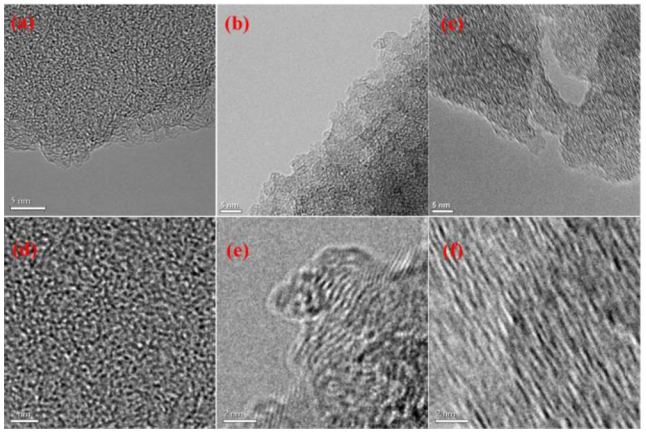

Figure 3. High magnification TEM images showing the edges (a, d) of CPANI, (b, e) CPANI-NaCl, and (c, f) CPANI-Fe-NaCl.

DOI: 10.1021/jacs.5b00292
J. Am. Chem. Soc. 2015, 137, 5414−5420

intensity ratio of G-band to D-band (I_G/I_D) for the CPANI-NaCl, implying that the graphitization degree of the CPANI-NaCl is higher than that of the CPANI. This is attributed to the effect of molten salts that promotes the degree of graphitization in the heat treatment process, which is consistent with the previous finding.[11] The clearest lattice fringe and the highest I_G/I_D, corresponding to CPANI-Fe-NaCl (Figure 3c,f, and Supporting Information Figure S5), indicate that the degree of graphitic structure can be further improved with the introduction of an Fe element.

TGA/DTA at a heating rate of 6 K min^{-1} in N_2 atmosphere was used to gauge how readily the precursors transform to carbon materials via the shape fixing via salt recrystallization method. As shown in Figure 4, PANI-NaCl exhibits excellent

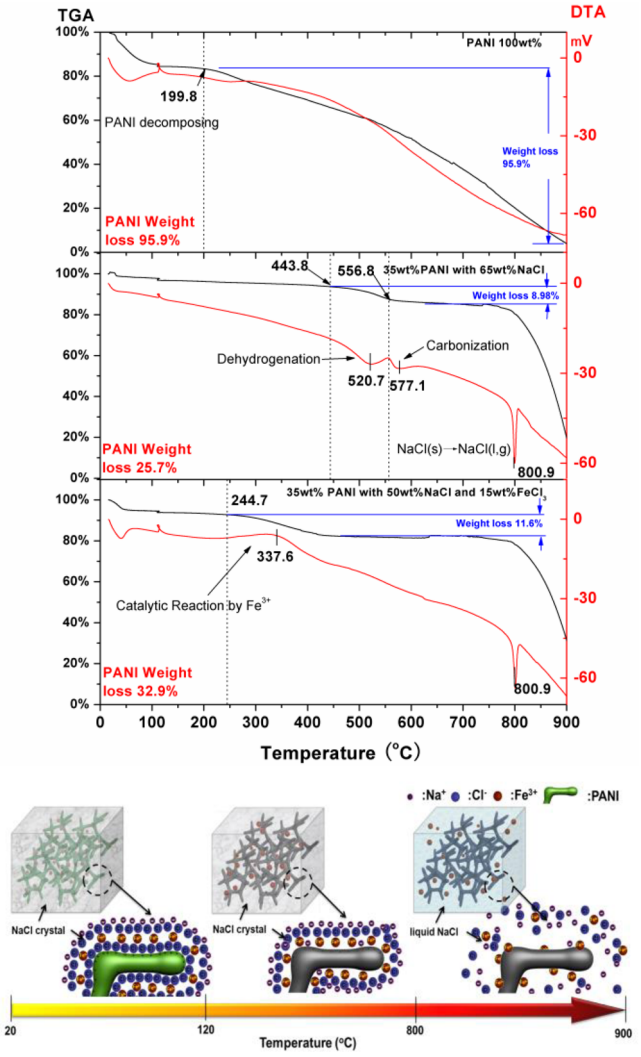

Figure 4. TGA-DTA plot of PANI, PANI-NaCl, and PANI-Fe-NaCl; and schematic of substance interactions during the synthesis.

thermal stability, with weight loss starting at 443.8 °C. The PANI, however, shows poor thermal stability. Its decomposition started at temperatures as low as 199.8 °C. At 900 °C, only 4.1% of the PANI residues remained, while 74.3% and 67.1% of the PANI-NaCl and PANI-Fe-NaCl residues remained, respectively. In addition, no obvious endothermic or exothermic processes were found in the PANI. Because of the uneven degree of the PANI polymerization, its decomposition (exothermic), dehydrogenation (endothermic), and carbonization (endothermic) may occur randomly and thus not occur at a certain temperature range. This result indicates a random transformation of PANI to carbon through direct pyrolysis. For PANI-NaCl, an endothermic process with weight loss was found at 520.7 °C, followed by the occurrence of another endothermic process without weight loss at 577.1 °C. The two endothermic processes are attributed to the dehydrogenation of PANI at the lower temperature and to the graphitization at the higher. With the addition of $FeCl_3$, only one exothermic process at 337.6 °C exhibited weight loss. One possible explanation is the catalytic effect of iron species during pyrolysis. The TGA/DTA plot of NaCl shows only one endothermic process at 800.9 °C corresponding to the melting of NaCl crystal (Supporting Information Figure S6). With the NaCl crystal melting at 800.9 °C, the graphitization of the pyrolyzed PANI was conducted in NaCl molten salts. It should be noted that the difference in the specific weights of NaCl molten salts (1.5 g cm^{-3}) and pyrolyzed PANI (1.8−2.1 g cm^{-3}) is too small to overcome the high viscosity of the NaCl molten salt, thereby avoiding phase separation. Therefore, the graphitization of the pyrolyzed PANI takes place inside the NaCl molten salts. As a matter of fact, as the samples cooled down to room temperature, the final carbon-based products were still sealed inside the NaCl crystal, just as shown in Scheme 1. The obvious weight loss after 800.9 °C in the TGA curve of Figure 4 comes from the vaporization of NaCl molten salts. As a result, the dehydrogenation, nitrogen doping, and graphitization of PANI, as well as the gasification of various additives in the present method, are always conducted in a sealed system. This will, at most, prevent weight loss and produce large quantities of pores in the final product, due to the trapped gas. As mentioned above, the invented method is conducive to increased active sites, induced by planar pyridinic N and pyrrolic N. The substance interactions and phase transitions may play important roles during the pyrolysis. The polyaniline is in a doped form. Its backbone carries positive charge.[12] Thus, during the absorption of $FeCl_3$, Cl^- ions will be preferentially adsorbed on the positively charged PANI, and then Fe^{3+} ions as shown in Figure 4. The outside of PANI-$FeCl_3$ was first covered by NaCl solution and then NaCl solids with the recrystallization of NaCl. The thick NaCl solid layer prevents the PANI from decomposition at a relatively lower temperature. With decomposition temperature increasing, the dedoping and dehydrogenation of PANI may finish before the PANI structure collapses. Nitrogen atoms with a lone pair electron are exposed to the outside with the dedoping and dehydrogenation of PANI. The exposed N reacts with Fe^{3+} ions, and forms a FeN_x/C complex. With the NaCl crystal melting at 800.9 °C, the excess Fe species are dissolved in molten NaCl and flow away from the surface. This will be beneficial for the active sites because too many Fe species would destroy them at high temperature.[13]

X-ray photoelectron spectroscopy (XPS) analysis was performed to investigate the content and chemical state of the nitrogen on the surface of the prepared catalysts. The existence of C−N and C−C (graphite-type) bonds in the matrix confirms the N-doped carbon structure of the prepared catalysts (see Supporting Information Figure S7). The relative N/C ratio was only 3.04% in CPANI but was 3.52% and 5.85% in CPANI-NaCl and CPANI-Fe-NaCl, respectively, indicating that nitrogen loss during pyrolysis at high temperatures was alleviated in the shape fixing via salt recrystallization method.

DOI: 10.1021/jacs.5b00292
J. Am. Chem. Soc. 2015, 137, 5414−5420

The high resolution N 1s spectra for all catalysts were fitted with five different signals, having binding energies of 398.6, 399.2, 400.3, 401.4, and ~403 eV, corresponding to pyridinic N, nitrile N, pyrrolic N, quaternary N, and oxidized pyridinic N, respectively (Supporting Information Figure S8). Pyridinic N (most likely including Me−N) and pyrrolic N are generally believed to activate neighboring carbon atoms for catalysis of the ORR.[9,14] As shown in Supporting Information Figure S8, the content of pyridinic and pyrrolic N in the CPANI-NaCl and the CPANI-Fe-NaCl is higher than that in CPANI, indicating that the shape fixing via salt recrystallization method is more suitable for facilitating more active-site formation. Besides, 11% of the N species in CPANI-NaCl are nitrile N, but no nitrile N is detected in CPANI-Fe-NaCl, indicating that the addition of iron species accelerates N incorporation into the carbon-ring. The CPANI species that have the highest content of quaternary N show the poorest activity for catalysis of the ORR in acidic medium. Supporting Information Figure S9 shows that Fe presents in the CPANI-Fe-NaCl as Fe^{3+} (3.18 atom %), which may exist as a stable complex form rather than simple inorganic ions because the CPANI-Fe-NaCl was treated in a hot H_2SO_4 solution. Na and Cl were not detected in the CPANI-Fe-NaCl after hot H_2SO_4 solution washing. This means that NaCl has been washed off by a hot solution. For CPANI-NaCl, Na and Cl were detected as a form of NaCl. This is because of the residual NaCl in the sample after room temperature water washing.

Electrical conductivity is a prominent concern for materials used in electrochemical applications. Electrochemical impedance spectroscopy (EIS) at high frequency (see the Supporting Information for details) revealed that the electrical resistance values of the CAPNI-NaCl and the CPANI-Fe-NaCl are on the same order as that of commercial Vulcan XC-72R carbon (Supporting Information Figure S10). In other words, the electrical conductivity of the CAPNI-NaCl and CPANI-Fe-NaCl is as good as that of commercial Vulcan XC-72R carbon. Conversely, CPANI and PANI demonstrate very poor electrical conductivity, as illustrated in Supporting Information Figure S10. These physical analysis data combined with TEM results demonstrate that NaCl preserves the original morphology of precursors and promotes the degree of graphitization, while iron species enhance both the graphitization and nitrogen incorporation during the synthesis.

The cyclic voltammograms (CVs) of CPANI and CPANI-NaCl in N_2-saturated H_2SO_4 solution are virtually featureless, while the CV of CPANI-Fe-NaCl reveals a pair of well-developed redox peaks at ~0.63 V versus the reversible hydrogen electrode (RHE) (see Supporting Information Figure S11). The peaks are expected for a reversible process involving surface Fe species (Fe^{3+} and Fe^{2+}). The Fe species are very stable. They cannot be removed by either acidic solution treatment at 80 °C or long-term electrochemical cycling in acidic solution (see Supporting Information Figure S14). The double layer capacities of the CPANI-Fe-NaCl and the CPANI-NaCl are similar to each other, but they are twice as large as that of CPANI. However, active sites of a metal catalyst can be examined by the CVs, but active sites of a nitrogen-doped carbon catalyst cannot. The CVs of the electrode made of nitrogen-doped carbon catalysts only tell the capacity of its electric double layer, which indicates the solid−electrolyte interface of the electrode but reveals nothing about the activity.

The activity of the catalysts was evaluated using a rotating ring−disk electrode (RRDE). All of the RRDE experiments were performed in 0.1 *m* $HClO_4$. The polarization curves and the Tafel slops for the catalysts are shown in Figure 5a and

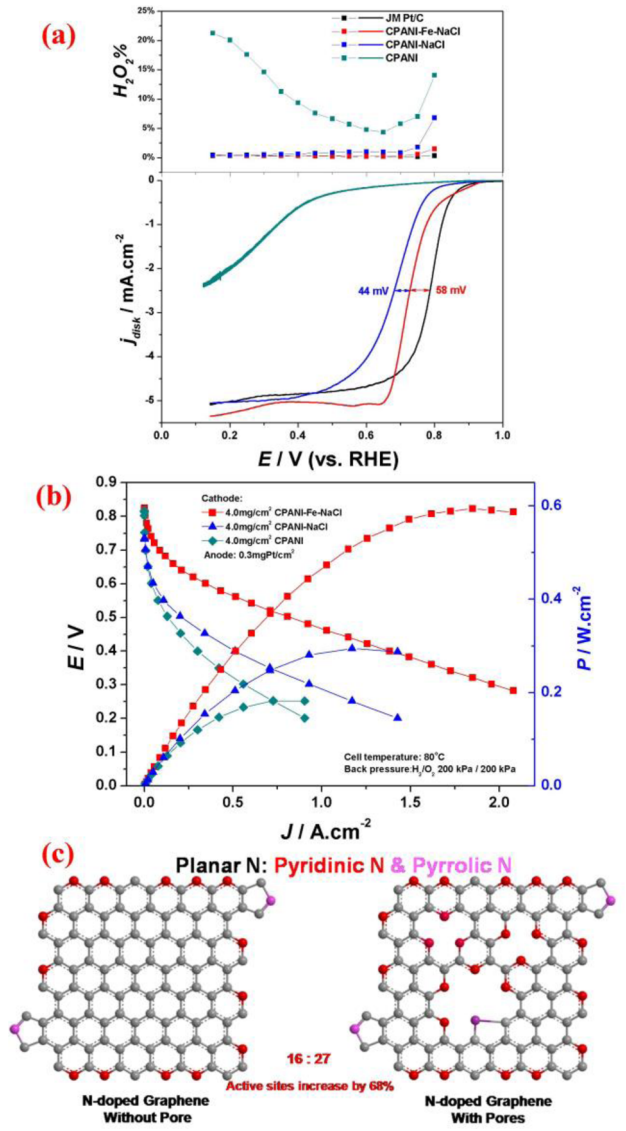

Figure 5. (a) Steady-state plots (bottom) of ORR polarization and (top) of H_2O_2 yield for different catalysts in O_2-saturated 0.1 *m* $HClO_4$. The loading is 50 μg of Pt cm^{-2} for Pt/C (40%) and is 0.6 mg cm^{-2} for non-Pt catalyst. (b) Polarization curves and corresponding power densities of membrane electrode assemblies fabricated with the CPANI-Fe-NaCl, CPANI-NaCl, and CPANI cathode catalysts. (c) Schematic of active sites on edges and in pores.

Supporting Information Figure S12, respectively. The CPANI-Fe-NaCl catalyst exhibited the highest activity, and the CPANI-NaCl metal-free catalyst also showed a good activity for the ORR. The ORR half-wave potentials measured on a CPANI-Fe-NaCl-catalyzed electrode and a CPANI-NaCl-catalyzed electrode were only 58 and 102 mV behind that from a state-of-the-art carbon-supported platinum catalyst (Johnson Matthey, 40 wt %, denoted as JM Pt/C) at a Pt loading of 50 μg Pt cm^{-2}. These results are comparable with those of the best NPMCs reported to date.[6b,9,15,16] The H_2O_2 yield was as low as 1.5% on a CPANI-Fe-NaCl-catalyzed electrode and 6.8% for a CPANI-NaCl-catalyzed electrode at the relative positive potential of 0.8 V (vs RHE). The H_2O_2 yield decreased with

DOI: 10.1021/jacs.5b00292
J. Am. Chem. Soc. 2015, 137, 5414−5420

a negative-shifting potential. At 0.5 V (vs RHE), it was only 0.28% on the CPANI-Fe-NaCl-catalyzed electrode and was 0.85% on the CPANI-NaCl-catalyzed electrode, which is comparable with that on the JM Pt/C electrode (0.30%). In any respect, CPANI exhibited poor activity for the ORR. The electron transfer number for the ORR on the CPANI-Fe-NaCl-catalyzed electrode was estimated according to the Koutecky–Levich plot. As shown in Supporting Information Figure S13, the electron transfer number is 3.9 ± 0.1 on the CPANI-Fe-NaCl-catalyzed electrode in the potential range 0.6–0.3 V, indicating a four-electron pathway for catalysis of the ORR and explaining the low H_2O_2 yield on the electrodes made of the prepared samples. The stability of the CPANI-Fe-NaCl- and CPANI-NaCl-catalyzed electrodes, together with the JM-Pt/C-catalyzed electrode, was assessed by cycling the electrodes in a potential range 0–1.2 V in N_2-saturated 0.5 M H_2SO_4 (see Supporting Information Figure S14). No noticeable change in catalytic activity of the ORR was observed on the CPANI-Fe-NaCl-catalyzed electrode, but the ORR half-wave potentials on the electrodes catalyzed by CPANI-NaCl and by JM Pt/C were negatively shifted by 27 and by 73 mV, respectively, after CV cycling, indicating the excellent stability of CPANI-Fe-NaCl but relatively poor stability of CPANI-NaCl and JM-Pt/C. The relatively poor stability of CPANI-NaCl is attributed to the existence of large numbers of nitrile species in the CPANI-NaCl, which may accelerate destruction of the catalyst under harsh conditions.

To investigate whether the remaining NaCl in CPANI-NaCl involves the ORR, the ORR activity of CPANI-NaCl was evaluated after repeated washes with hot water until no Cl^- was detected. As shown in Supporting Information Figure S15, the activities appear to be unchanged after removal of NaCl, indicating that NaCl does not involve the catalysis of the ORR. As mentioned above, Fe species are hardly removed from the CPANI-Fe-NaCl, even by being treated in a hot acidic solution or by being long-term cycled in acidic solution (Supporting Information Figure S14a). This suggests that Fe elements may exist in a very stable complex rather than as simple inorganic ions; otherwise, Fe would be leached off from the catalysts. According to recent studies that relied on Mössbauer spectroscopy and X-ray absorption spectroscopy about the Fe state after pyrolysis of the mixture of PANI and iron-containing species, Fe elements exist in a FeN_x/C complex, of which FeN_4/C and N-FeN_{2+2}/C are highly active for the ORR in acid medium.[17] In contrast, some argued that Fe only promotes key properties of the catalyst, such as electronic conductivity, morphology, and nitrogen-doping level, but it does not directly participate in the active site.[18] We made a comparative investigation between Fe-free and Fe-doping catalyst, that is, CPANI-NaCl and CPANI-Fe-NaCl. Our results show that their electronic conductivity, morphology, and nitrogen-doping level are quite similar to each other but their ORR activities are different. As shown in Figure 5a, the electrode made of the CPANI-NaCl catalysts (Fe-free) shows excellent ORR activity, indicating the nitrogen-doped carbon without Fe also catalyzes the ORR. This is ascribed to numerous inner pores formed in the present method. The sites activated by planar pyridinic and pyrrolic N atoms with sp^2 hybrid orbitals, which appear at the fringes of a graphene sheet and the fringes of graphene inner pores, are active for the ORR. The present method makes such active sites obviously increase, for instance, 68% for the given graphene sheet as shown in Figure 5c. On the other hand, the electrode made of the CPANI-Fe-NaCl catalysts (Fe-doping) shows much better ORR activity. The catalytic role of the Fe complex for the ORR is obvious, which is in accordance with previous studies based on Mössbauer spectroscopy.[15a,19] According to Frédéric Jaouen's research result, the Fe/N/C-catalyst contains two types of FeN_x sites assigned to micropore-hosted sites in edges and graphene-defect-hosted sites in the inner plane, while the latter are more stable than the former during the carbon corrosion.[19] The present method might benefit from more FeN_x-site formation owing to the existence of numerous inner pores, as shown in Supporting Information Figure S19. At this stage, we cannot exclude another role for the Fe species in improving graphitic structure, which is well-known to be conducive for the catalysis of the ORR as reported before.[9,15,19]

The performance of the single cell with these catalyst-based cathodes and Pt/C anodes is shown in Figure 5b. An open-circuit voltage (OCV) of 0.85 V was observed, and the current density reached as high as 2.1 A cm^{-2} at 0.28 V. A higher OCV of 0.9 V was observed when the MEA was prepared using Nafion 117 to substitute for Nafion 112 to reduce the crossover current (see Supporting Information Figure S16). A maximum power output of 600 mW cm^{-2} was achieved with the CPANI-Fe-NaCl-catalyzed cathode, with 300 mW cm^{-2} for the metal-free, CPANI-NaCl-catalyzed cathode. In contrast, the maximum power output is only 180 mW cm^{-2} for the CPANI-catalyzed cathode, which is consistent with the previous report about the single cell performance of an NC-catalyzed cathode obtained from directly pyrolyzed PANI.[16] The CPANI-Fe catalyst produced without NaCl also shows a poor performance with the maximum power output of only 284 mW cm^{-2} (Supporting Information Figure S17). This reveals that NaCl participation is very important in synthesis of highly active nitrogen-doped carbon catalysts.

In the present work, the loading of nitrogen-doped carbon catalysts in the catalyst layer is much higher than that of Pt catalysts, 4.0 mg cm^{-2} versus 0.1 or 0.3 mg cm^{-2}. Thus, the ohmic voltage loss in the catalyst layer is not negligible owing to the thick catalyst layer but is negligible in the case of Pt/C catalysts owing to its ultrathin catalyst layer. The ohmic resistance would affect the $I-V$ slope. As shown in Figure 5b, the $I-V$ slopes of the three types of catalysts are different from each other. The $I-V$ slopes indicate the electric resistance of the three types of cathodes, that is, $R_{\text{CPANI-Fe-NaCl}} \approx R_{\text{CPANI-NaCl}} \ll R_{\text{CPANI}}$. This is consistent with the EIS result illustrated in Supporting Information Figure S10.

An internal comparison has been made with the commercial Pt/C catalyst. As shown Supporting Information Figure S17, with the JM Pt/C-catalyzed cathodes, the maximum power output is 450 mW cm^{-2} at Pt loading of 0.1 mg cm^{-2} and is 820 mW cm^{-2} at 0.3 mg Pt cm^{-2}. The CPANI-Fe-NaCl with the maximum power output of 600 mW cm^{-2} shows a performance comparable to that of the commercial Pt/C. In addition, the single cell performances of the different morphology CPANI-Fe-NaCl-catalyzed cathodes are evaluated as shown in Supporting Information Figure S18. The maximum power output is 530 mW cm^{-2} with the nanotube CPANI-Fe-NaCl-catalyzed cathode, and is 490 mW cm^{-2} with the nanoshell CPANI-Fe-NaCl-catalyzed cathode. The cell performances observed in these tests are among the best reported worldwide, to date.[6] In contrast to efforts that focus on improving the surface area, the best catalyst found in the present work has a BET surface area of only 265.7 m^2 g^{-1}, but exhibits excellent cell performance despite this. This is attributed to the unique

DOI: 10.1021/jacs.5b00292
J. Am. Chem. Soc. 2015, 137, 5414–5420

advantages of the shape fixing via salt recrystallization method, by which a high microporosity is achieved, with a high density of ORR active sites located along the efficient mass-transport pathway (composed of meso- and macropores), leading to a high utilization of active sites.

CONCLUSION

In summary, we have demonstrated a shape fixing via salt recrystallization method to efficiently synthesize N-doped carbon nanomaterials with a high density of active sites, as an ORR catalyst. In this method, the NaCl crystal functions as a fully sealed nanoreactor, facilitating the N incorporation and graphitization. The gas from gasification in such a closed nanoreactor produces a large quantity of pores in resultant samples. As for an Fe-free catalyst, this method makes it possible for the active sites (activated by planar pyridinic and pyrrolic N atoms with sp^2 hybrid orbitals, which only appear at the outside fringe of a graphene sheet) to appear in large quantities on the edges of numerous pores, as shown in Figure 5c. As for an Fe-doping catalyst, the present method benefits formation of more FeN_x sites in inner pores and graphitic structure. A favorable catalyst structure leads to the availability of efficient mass-transport pathways and a high utilization of the active sites. It results in an excellent ORR activity with a half-wave potential only 58 mV behind that of Pt/C in an acidic medium. The PEMFC with the CPANI-Fe-NaCl-catalyzed cathode has a peak power output of 600 mW cm^{-2}, which is among the best for nonprecious metal catalysts reported so far for the ORR. Additionally, no other method is comparable to this invention, in terms of its high yield per batch of N-doped carbon catalysts. The shape fixing via salt recrystallization method represents a powerful approach for the preparation of high performance carbon nanostructures by confined pyrolysis of nanopolymers and, more importantly, provides insight into the design of advanced PEMFC cathode catalysts.

ASSOCIATED CONTENT

Supporting Information

Experimental details and more characterization and results. This material is available free of charge via the Internet at http://pubs.acs.org.

AUTHOR INFORMATION

Corresponding Author

*zdwei@cqu.edu.cn

Notes

The authors declare no competing financial interest.

ACKNOWLEDGMENTS

This work was financially supported by the China National 973 Program (2012CB720300 and 2012CB215500), by the NSFC of China (Grants 21436003 and 51272297).

REFERENCES

(1) (a) Gasteiger, H. A.; Markovic, N. M. *Science* **2009**, *324*, 48. (b) Strasser, P.; Koh, S.; Anniyev, T.; Greeley, J.; More, K.; Yu, C.; Liu, Z.; Kaya, S.; Nordlund, D.; Ogasawara, H.; Toney, M. F.; Nilsson, A. *Nat. Chem.* **2010**, *2*, 454. (c) Wang, C.; Vliet, D.; More, K. L.; Zaluzec, N. J.; Peng, S.; Sun, S.-H.; Daimon, H.; Wang, G.-F.; Greeley, J.; Pearson, J.; Paulikas, A. P.; Karapetrov, G.; Strmcnik, D.; Markovic, N. M.; Stamenkovic, V. R. *Nano Lett.* **2010**, *11*, 919. (d) Wu, J.; Zhang, J.; Peng, Z.; Yang, S.; Wagner, F. T.; Yang, H. *J. Am. Chem. Soc.* **2010**, *132*, 4984.

(2) (a) Bezerra, C. W. B.; Zhang, L.; Lee, K.; Liu, H.; Marques, A. L. B.; Marques, E. P.; Zhang, J. *Electrochim. Acta* **2008**, *53*, 4937. (b) Lefevre, M.; Proietti, E.; Jaouen, F.; Dodelet, J-P. *Science* **2009**, *324*, 71. (c) Pylypenko, S.; Mukherjee, S.; Olson, T. S.; Atanassov, P. *Electrochim. Acta* **2008**, *53*, 7875.

(3) Jaouen, F.; Proietti, E.; Lefèvre, M.; Chenitz, R.; Dodelet, J.-P.; Wu, G.; Zelenay, P. *Energy Environ. Sci.* **2011**, *4*, 114.

(4) (a) Yang, S.-B.; Feng, X.-L.; Wang, X.-C.; Müllen, K. *Angew. Chem.* **2011**, *50*, 5339. (b) Rao, C.-V.; Cabrera, C.-R.; Ishikawa, Y. *J. Phys. Chem. Lett.* **2010**, *1*, 2622. (c) Wang, X. B.; Liu, Y. Q.; Zhu, D. B.; Zhang, L.; Ma, H. Z.; Yao, N.; Zhang, B. L. *J. Phys. Chem. B* **2002**, *106*, 2186.

(5) Serov, A.; Artyushkova, K.; Atanassov, P. *Adv. Energy Mater.* **2014**, *4*, 1301735.

(6) (a) Proietti, E.; Jaouen, F.; Lefevre, M.; Larouche, N.; Tian, J.; Herranz, J.; Dodelet, J. P. *Nat. Commun.* **2011**, *2*, 416. (b) Yuan, S.-W.; Shui, J.-L.; Grabstanowicz, L.; Chen, C.; Commet, S.; Reprogle, B.; Xu, T.; Yu, L. P.; Liu, D. J. *Angew. Chem., Int. Ed.* **2013**, *52*, 8349. (c) Tian, J.; Morozan, A.; Sougrati, M. T.; Lefèvre, M.; Chenitz, R.; Dodelet, J.-P.; Jones, D.; Jaouen, F. *Angew. Chem., Int. Ed.* **2013**, *52*, 6867.

(7) (a) Wei, Z.-D.; Chen, S. G.; Liu, Y.; Sun, C. X.; Shao, Z. G.; Shen, P. K. *J. Phys. Chem. C* **2007**, *42*, 15456. (b) Zhang, H.; Wang, X.; Zhang, J.; Zhang, J. In *PEM Fuel Cell Electrocatalysts and Catalyst Layers*; Zhang, J., Ed.; Springer: London, 2008, p 889.

(8) (a) Ignaszak, A.; Ye, S.; Gyenge, E. *J. Phys. Chem. C* **2008**, *113*, 298. (b) Antolini, E. *Appl. Catal., B* **2009**, *88*, 1.

(9) Ding, W.; Wei, Z.-D.; Chen, S. G.; Qi, X. Q.; Yang, T.; Hu, J.-S.; Wang, D.; Wan, L.-J.; Alvi, S. F.; Li, L. *Angew. Chem., Int. Ed.* **2013**, *52*, 11755.

(10) Zhang, L. J.; Wan, M. X. *Adv. Funct. Mater.* **2003**, *13*, 815.

(11) Kamali, A. R.; Fray, D. J. *Carbon* **2013**, *56*, 121.

(12) Wang, Y.; Guan, X. N.; Wu, C.-Y.; Chen, M.-T.; Hsieh, H.-H.; Tran, H. D.; Huang, S.-C.; Kaner, R. B. *Polym. Chem.* **2013**, *4*, 4814.

(13) (a) Nabae, Y.; Moriya, S.; Matsubayashi, K.; Lyth, S. M.; Malon, M.; Wu, L.; Islam, N. M.; Koshigoe, Y.; Kuroki, S.; Kakimoto, M.; Miyata, S.; Ozaki, J. *Carbon* **2010**, *48*, 2613. (b) Wu, L.-B.; Nabae, Y.; Moriya, S.; Matsubayashi, K.; Islam, N. M.; Kuroki, S.; Kakimoto, M.; Ozaki, J.; Miyata, S. *Chem. Commun.* **2010**, *46*, 6377.

(14) (a) Yu, D. S.; Zhang, Q.; Dai, L. M. *J. Am. Chem. Soc.* **2010**, *132*, 15127. (b) Liu, G.; Li, X. G.; Ganesan, P.; Popov, B. N. *Electrochim. Acta* **2010**, *55*, 2853. (c) Liu, G.; Li, X. G.; Lee, J. W.; Popov, B. N. *Catal. Sci. Technol.* **2011**, *1*, 207. (d) Liang, Y.; Li, Y.; Wang, H.; Zhou, J.; Wang, J.; Regier, T.; Dai, H. *Nat. Mater.* **2011**, *10*, 780. (e) Wang, S.; Zhang, L.; Xia, Z.; Roy, A.; Chang, D.-W.; Baek, J.-B.; Dai, L. *Angew. Chem.* **2012**, *51*, 4209.

(15) Liang, H.-W.; Wei, W.; Wu, Z.-S.; Feng, X. l.; Müllen, K. *J. Am. Chem. Soc.* **2013**, *135*, 16002.

(16) Wu, G.; More, K. L.; Johnston, C. M.; Zelenay, P. *Science* **2011**, *332*, 443.

(17) (a) Kramm, U. I.; Lefevre, M.; Larouche, N.; Schmeisser, D.; Dodelet, J.-P. *J. Am. Chem. Soc.* **2014**, *136*, 978. (b) Kramm, U. I.; Herranz, J.; Larouche, N.; Arruda, T. M.; Lefevre, M.; Jaouen, F.; Bogdanoff, P.; Fiechter, S.; Abs-Wurmbach, I.; Mukerjee, S.; Dodelet, J.-P. *Phys. Chem. Chem. Phys.* **2012**, *14*, 11673. (c) Zhang, S. M.; Liu, B.; Chen, S. L. *Phys. Chem. Chem. Phys.* **2013**, *15*, 18482.

(18) (a) Nallathambi, V.; Lee, J. W.; Kumaraguru, S. P.; Wu, G.; Popov, B. N. *J. Power Sources* **2008**, *183*, 34. (b) Woods, M. P.; Biddinger, E. J.; Matter, P. H.; Mirkelamoglu, B.; Ozkan, U. S. *Catal. Lett.* **2010**, *136*, 1.

(19) Goellner, V.; Baldizzone, C.; Schuppert, A.; Sougrati, M. T.; Mayrhofer, K.; Jaouen, F. *Phys. Chem. Chem. Phys.* **2014**, *16*, 18454.

DOI: 10.1021/jacs.5b00292
J. Am. Chem. Soc. 2015, 137, 5414−5420